Spatio-temporal reshaping and X Wave dynamics in optical filaments.

D. Faccio[1], A. Averchi[1], A. Couairon[2], M. Kolesik[3], J.V. Moloney[3], A. Dubietis[4], G. Tamosauskas[4], P. Polesana[4], A. Piskarskas[4], P. Di Trapani[1,4]

[1]*CNISM and Department of Physics and Mathematics, University of Insubria, Via Valleggio 11, IT-22100 Como, Italy*
[2]*Centre de Physique Théorique, CNRS, École Polytechnique, F-91128, Palaiseau, France*
[3]*Arizona Center for Mathematical Sciences and Optical Sciences Center, University of Arizona, Tucson, 85721 AZ, U.S.A.*
[4]*Department of Quantum Electronics, Vilnius University, Saulėtekio Ave. 9, bldg.3, LT-10222 Vilnius, Lithuania.*
daniele.faccio@uninsubria.it

Abstract: We investigate ultrashort laser pulse filamentation within the framework of spontaneous X Wave formation. After a brief overview of the filamentation process we study the case of an intense filament co-propagating with a weaker seed pulse. The filament is shown to induce strong Cross-Phase-Modulation (XPM) effects on the weak seed pulse: driven by the pump, the seed pulse undergoes pulse splitting with the daughter pulses slaved to their pump counterparts. They undergo strong spatio-temporal reshaping and are transformed into X Waves traveling at the same group velocities as the pump split-off pulses. In the presence of a gain mechanism such as Four-Wave-Mixing or Stimulated Raman Scattering, energy is then transferred from the pump filament leading to amplification of the seed X Wave and formation of a temporally compressed intensity peak.

OCIS codes: (190.5940) Self-action effects; (320.2250) Femtosecond phenomena; (190.5890) Scattering, stimulated.

References and links

1. A. Couairon and A. Mysyrowicz, Femtosecond filamentation in transparent media, Phys. Rep. **441**, 47-189 (2007).
2. R.R. Alfano, "The Supercontinuum Laser Source," Springer-Verlag, New York (1989).
3. P. Rairoux, H. Schillinger, S. Niedermeier, M. Rodriguez, F. Ronneberger, R. Sauerbrey, B.Stein, D. Waite, C. Wedekind, H. Wille, L. Wöste, and C.Ziener, "Remote sensing of the atmosphere using ultrashort laser pulses," Appl. Phys. B **71**, 573-580 (2000)
4. M. Rodriguez, R. Sauerbrey, H. Wille, L. Wöste, T. Fujii, Y.B. André, A. Mysyrowicz, L. Klingbeil, K. Rethmeier, W. Kalkner, J. Kasparian, E. Salmon, J. Yu, and J.P. Wolf, "Triggering and guiding megavolt discharges by use of laser-induced ionized filaments," Opt. Lett. **27**, 772-774 (2002)
5. F. Théberge, N. Aközbek , W. Liu, A. Becker, and S. L. Chin, "Tunable Ultrashort Laser Pulses Generated through Filamentation in Gases," Phys. Rev. lett. **97**, 023904 (2006)
6. S. L. Chin, F. Théberge, and W. Liu , "Filamentation nonlinear optics," Appl. Phys. B **86**, 477-483 (2007)
7. D. Faccio, A. Averchi, A. Dubietis, P. Polesana, A. Piskarskas, P. Di Trapani and A .Couairon, "Stimulated-Raman X Waves in Ultrashort Optical Pulse Filamentation," Opt. Lett. **32,** 184–186 (2007)
8. M. Kolesik, E.M. Wright and J.V. Moloney, "Dynamic Nonlinear X Waves for Femtosecond Pulse Propagation in Water," Phys. Rev. Lett. **92**, 253901 (2004).

#83915 - $15.00 USD Received 7 Jun 2007; revised 23 Jul 2007; accepted 24 Sep 2007; published 26 Sep 2007

9. D. Faccio, M. A. Porras, A. Dubietis, F. Bragheri, A. Couairon, and P. Di Trapani, "Conical Emission, Pulse Splitting, and X Wave Parametric Amplification in Nonlinear Dynamics of Ultrashort Light Pulses," Phys. Rev. Lett. **96**, 193901 (2006).
10. H. Sõnajalg, M. Rätsep, and P. Saari, "Demonstration of the Bessel-X pulse propagating with strong lateral and longitudinal localization in a dispersive medium," Opt. Lett. **22**, 310-312 (1997).
11. C. Conti, S. Trillo, P. Di Trapani, G. Valiulis, A. Piskarskas, O. Jedrkiewicz, and J. Trull, "Nonlinear electromagnetic X Waves," Phys. Rev. Lett. **90**, 170406 (2003).
12. K. D. Moll, A.L. Gaeta, and G. Fibich, "Self-Similar Optical Wave Collapse: Observation of the Townes Profile", Phs, Rev. Lett., **90** 203902 (2004)
13. V. Sirutkaitis, E.Gaižauskas, V.Kudriašov, M.Barkauskas, R. Grigonis, V. Vaičaitis, and A.Piskarskas, "Self-guiding, supercontinuum generation and damage in bulk materials induced by femtosecond pulses," SPIE Proc. **4932**, 346357 (2003).
14. A. Dubietis, E. Gaižauskas, G. Tamošauskas and Paolo Di Trapani, "Light filaments without self channeling," Phys. Rev. Lett., **92** 252903 (2004).
15. A. Couairon, E. Gaižauskas, D. Faccio, A. Dubietis and P. Di Trapani, "Nonlinear X-wave formation by femtosecond filamentation in Kerr media," Phys. Rev. E **73**, 016608 (2006).
16. M.A. Porras, A. Parola, D. Faccio, A. Couairon and P. Di Trapani, "Light-filament dynamics and the spatiotemporal instability of the Townes profile," Phys. Rev. A, **76** 011803 (2007).
17. C. Conti, "Generation and nonlinear dynamics of X Waves of the Schrodinger equation," Phys. Rev. E **70**, 046613 (2004).
18. G.P. Agrawal, "Nonlinear fiber optics," Academic Press Inc., New York (1989).
19. B. Prade, M. Franco, A. Mysyrowicz, A. Couairon, H. Buersing, B. Eberle, M. Krenz, D. Seiffer and O. Vasseur, "Spatial Mode Cleaning by Femtosecond Filamentation in air," Opt. Lett. **31**, 2601-2603 (2007).
20. T. Pfeifer, L. Gallmann, M. J. Abel, D. M. Neumark, and S. R. Leone, "Stationary phase-mask for control and stabilization of optical filaments," Opt. Lett. **31**, 2326-2328 (2006).
21. C. P. Hauri, W. Kornelis, F. W. Helbing, A. Heinrich, A. Couairon, A. Mysyrowicz, J. Biegert, U. Keller, "Generation of intense, carrier-envelope phase-locked few-cycle laser pulses through filamentation," Appl. Phys. B **79**, 673-677 (2004).
22. A. Couairon, J. Biegert, C. P. Hauri, W. Kornelis, F. W. Helbing, U. Keller, and A. Mysyrowicz, "Self-compression of ultra-short laser pulses down to one optical cycle by filamentation," J. Mod. Optics **53**, 75-85 (2006).
23. A. Guandalini, P. Eckle, M. P. Anscombe, P. Schlup, J. Biegert, and U. Keller, "5.1 fs pulses generated by filamentation and carrier-envelope phase stability analysis," J. Phys. B: At. Mol. Opt. Phys. **39**, S257-S264 (2006).
24. A. Zaïr, A. Guandalini, F. Schapper, M. Holler, J. Biegert, L. Gallmann, U. Keller, A. Couairon, M. Franco, and A. Mysyrowicz, "Spatio-temporal characterization of few-cycle pulses obtained by filamentation", Opt. Express **15**, 5394-5405 (2007).
25. A. Couairon, M. Franco, A. Mysyrowicz, J. Biegert, and U. Keller, "Pulse self-compression to the single cycle limit by filamentation in a gas with a pressure gradient," Opt. Lett, **30**, 2657-2659 (2005).
26. H. S. Chakraborty, M. B. Gaarde, and A. Couairon, "Single attosecond pulses from high harmonics driven by self-compressed filaments," Opt. Lett. **31**, 3662-3664 (2006).
27. P. B. Corkum and F. Krausz, "Attosecond Science", Nature Physics **3**, 381-387 (2007).
28. D. Faccio, P. Di Trapani, S. Minardi, A. Bramati, F. Bragheri, C. Liberale, V. Degiorgio, A. Dubietis, A. Matijosius, "Far-field spectral characterization of conical emission and filamentation in Kerr media," J. Opt. Soc. Am. B **22**, 862–869 (2005).
29. M. Kolesik, E.M. Wright, and J.V. Moloney, "Interpretation of the spectrally resolved far field of femtosecond pulses propagating in bulk nonlinear dispersive media," Opt. Express **13**, 10729–10741 (2005).
30. M. Wittmann and A. Penzkofer, "Spectral superbroadening of femtosecond laser pulses," Opt. Commun. **126**, 308–317 (1996).
31. D. Faccio, A. Averchi, A. Couairon, A. Dubietis, R. Piskarskas, A. Matijosius, F. Bragheri, M. A. Porras, A. Piskarskas, and P. Di Trapani, "Competition between Phase-matching and stationarity in Kerr-driven optical pulse filamentation," Phys. Rev. E **74**, 047603 (2006).
32. Commercial CCD cameras come equipped with a limiting spectral filter in front of the CCD. This may be removed and substituted with a clear glass. For more details see http://www.lifepixel.com/IR.htm.
33. A.G. Van Engen, S.A. Diddams, and T.S. Clement, "Dispersion measurements of water with white-light interferometry," Appl. Opt. **37**, 5679–5686 (1998).
34. M. Kolesik, J. V. Moloney and M. Mlejnek, "Unidirectional Optical Pulse Propagation Equation," Phys. Rev. Lett. **89**, 283902 (2002).
35. M. Kolesik and J. V. Moloney, "Nonlinear optical pulse propagation simulation: From Maxwell's to unidirectional equations," Phys. Rev. E **70**, 036604 (2004).
36. S. Trillo, C. Conti, P. Di Trapani. O. Jedrkiewicz, J. Trull, G. Valiulis and G. Bellanca, "Coloured conical emission via second-harmonic generation," Opt. Lett., **27**, 1451–1453 (2002).
37. D. Faccio, A. Matijosius, A. Dubietis, R. Piskarkas, A. Varanavicius, E. Gaizauskas, A. Piskarkas, A. Couairon

#83915 - $15.00 USD Received 7 Jun 2007; revised 23 Jul 2007; accepted 24 Sep 2007; published 26 Sep 2007

and P. Di Trapani, "Near and Far-Field evolution of laser pulse filaments in Kerr media," Phys. Rev. E, **72**, 037601 (2005)
38. O. Jedrkiewicz, J. Trull, G. Valiulis, A. Piskarskas, C. Conti, S. Trillo, and P. Di Trapani, "Nonlinear X waves in second-harmonic generation: Experimental results," Phys. Rev. E, **68**, 0266101-12 (2003).
39. M. Kolesik, G. Katona, J.V. Moloney, and E.M. Wright, "Theory and simulation of supercontinuum generation in transparent bulk media," Appl. Phys. **B77**, 185-195 (2003).
40. M. Uiberacker et al., "Attosecond real-time observation of electron tunneling in atoms," Nature **446**, 627-632 (2007).
41. L. Gallmann, T. Pfeifer, P. M. Nagel, M. J. Abel, D. M. Neumark, and S .R. Leone, "Comparison of the filamentation and the hollw-core fiber characteristics for pulse compression into the few-cycle regime" App. Phys. B. **86**, 2503-2508 (2007).
42. M. B. Gaarde, H. Chakraborty, and A. Couairon, "An alternative source of isolated attosecond light pulses," SPIE Newsroom 10.1117/2.1200706.0619 (2007).
43. A. Couairon, G. Méchain, S. Tzortzakis, M. Franco, B. Lamouroux, B. Prade and A. Mysyrowicz, "Propagation of twin laser pulses in air and concatenation of plasma strings produced by femtosecond infrared filaments," Opt. Commun. **225**, 177-192 (2003).
44. A. Dubietis, R. Butkus, and A. Piskarskas, "Trends in chirped pulse optical parametric amplification," IEEE J. Sel. Top. Quantum Electron. **12**, 163-172 (2006).
45. N. Ishii, L. Turi, V. S. Yakovlev, T. Fuji, F. Krausz, A. Baltuška, R. Butkus, G. Veitas, V. Smilgevičius, R. Danielius, and A. Piskarskas "Multimillijoule chirped parametric amplification of few-cycle pulses," Opt. Lett. **30**, 567-569 (2005).

1. Introduction

Ultrashort laser pulse filamentation is an extremely rich branch of nonlinear optics that has been attracting interest for many years now [1] due to both the fundamental physical implications and the potential applications ranging from spectral superbroadening [2] and remote sensing [3], lightning protection [4] and, more recently, frequency conversion [5, 6, 7]. It has also been shown that the filament dynamics in condensed media with normal group velocity dispersion (GVD) may be understood in terms of spontaneous formation and successive interaction of nonlinear X-waves [8, 9]. X Waves, or more generically, conical waves, are particular solutions of the propagation equation with the notable feature of being stationary, i.e. non-dispersive and non-diffractive, in both the linear (low intensity) [10] and nonlinear (high intensity) [11] regimes. Therefore, ultrashort laser pulse filamentation may be viewed as a highly dynamical interaction between spontaneously generated conical waves, where an asymptotically linear, stationary state serves as an attractor providing the driving force for the pulse evolution. Within this framework, the initial filamentation stage is dominated by self-focusing and in particular by a self-similar collapse of the Townes profile [12]. The collapse process will eventually be arrested typically by nonlinear losses (NLL) [13, 14, 15] or by self-induced plasma defocusing [1], depending on the specific material and operating conditions. It is known that the Townes profile is a stationary yet unstable solution to the nonlinear Schrödinger propagation equation and, indeed, close to the tightest focus point the peak intensities reached by the pulse are such that they excite and amplify strong spatio-temporal instabilities [16]. It has been shown that the angular spectra of the corresponding unstable modes will evolve into X-shaped spectra [16]. Propagation immediately after the nonlinear focus may then be described in different manners, for example based on the numerical solution of the nonlinear propagation equation [8], in terms of a parametric generation and amplification of X Waves [9] or by describing the nonlinear X Wave dynamics in terms of a 1D NLSE with a non-uniform nonlinearity profile [17]. All these approaches agree on the fact that the nonlinear dynamics are dominated by a pulse splitting event, i.e. a generation of two daughter X Waves that travel with opposite group velocities (in the reference frame moving at the input gaussian pulse group velocity). In the far-field spectra clear X-shaped spectra that are well described in terms of stationary X Wave spectra are formed and remain largely unvaried during further propagation, thus suggesting that the newly formed nonlinear X-waves have the same spectral signature as that of stationary

#83915 - $15.00 USD Received 7 Jun 2007; revised 23 Jul 2007; accepted 24 Sep 2007; published 26 Sep 2007

X-waves. For high enough energies these two X Waves will continue to interact nonlinearly leading to a dynamical replenishment of the central peak and eventually to a new splitting event [8]. This dynamical process may occur cyclicly and has even been interpreted in terms of a "breathing X Wave", in close analogy with breathing solitons [17]. In the last stage of the filament the overlap between the conical components of the X Waves will be strongly reduced, the peak intensity will start to decrease and diffraction will set in, in a very similar fashion to what is observed with linear Bessel Beams approaching the end of the so-called Bessel zone. We underline that the description of ultrashort laser pulse filamentation in terms of X Wave formation goes beyond the over-simplified idea that single, stationary, X Waves are formed and is based on the observation that, due to the extremely high intensities involved, the X Waves continuously interact within the filament leading to a highly dynamical propagation. This is not in contradiction with the interpretation of the physics in terms of a basis of stationary states and indeed the filamentation process finds an accurate description in terms of X Wave formation and interaction as shown in literature and in the present work.

The above described dynamics typically do not involve the whole input pulse but the only a small portion of the overall energy corresponding to the higher intensity regions while the weaker outer regions of the pulse will continue to propagate in a linear fashion. This immediately implies that a direct spatio-temporal characterization of the near-field reveals complicated interference patterns between the two regions [37] and to date, a clear space-time measurement of the X Waves contained within the filament is still lacking. However we note that the tightly focused X Wave features in the near-field become extended, extremely visible and background-free features in the Fourier domain. This is the key feature of the characterization method used in this work and described in detail below.

Optical filaments also exhibit certain features that render them very attractive for efficient frequency conversion, opening the possibility for what may be called "nonlinear filamentation optics" [6]. The main features motivating this interest may be listed as:

1) High intensities over very large propagation distances; On the contrary to the behavior of Gaussian pulses, the high ($\sim$ TW/cm^2 in condensed media) intensity peaks, that form within a filament, propagate without diffraction over many Rayleigh lengths. This drastically increases the efficiency of many nonlinear processes in a way very similar to what observed in optical fibers [18].

2) The drastic improvement in beam quality and energy stability of newly generated frequencies [6, 19, 20] promises an increase in pulse quality, in contrast to the reduction of pulse quality usually encountered, for example, in standard (i.e. based on Gaussian beams) parametric generators.

Clearly, detailed understanding of the dynamics that controls the ultrashort pulse interactions with media is necessary to take advantage of these properties in practical applications. The present paper is a result of our efforts in this direction. We study femtosecond filamentation in condensed media (water, ethanol) in situations where a high-power pulse (pump) interacts with a relatively weak "seed" pulse. Our goal is to analyze in detail, both numerically and experimentally, the role of various nonlinear effects, namely Cross-Phase-Modulation (XPM), Four-Wave Mixing (FWM) and Stimulated Raman Scattering (SRS) that concur to modify the spatio-temporal profile of a weak seed pulse in the presence of a high intensity optical filament.

More specifically, we will show that there is a hierarchy of nonlinear processes that control the spatial and temporal reshaping of the seed and pump pulses. We identify three classes or levels of nonlinear interactions that, taken together, provide a complete and coherent picture of the two-color filamentation: the basic process is first the formation of X Waves (or, in general, conical wave) around the central frequencies of both, pump and seed pulses. Next, a more complicated process controls the evolution in case of resonance, e.g. when the detuning between

#83915 - $15.00 USD Received 7 Jun 2007; revised 23 Jul 2007; accepted 24 Sep 2007; published 26 Sep 2007

pump and seed corresponds to the SRS frequency shift. Here, the resulting seed-centered X Waves are very efficiently "amplified" due to the resonant energy transfer by SRS. Finally, at the third level we encounter a whole family of FWM-type effects in which one of the incoming waves is an X Wave. The reason why all these processes occur with high efficiency is that group velocity matching occurs *in a natural way at each level*.

We also demonstrate that the above mentioned nonlinear interactions can produce self-compressed pulses. Filamentation in gases is already known as generating self-compressed few-cycle pulses in constant pressure argon cells [21, 22, 23, 24] . Enhancement of the compression ratio of 8 (from 40 to 5 fs) was shown to be possible by using a variable gas density [25]. In the present two-color filamentation scheme in liquids, we demonstrate extreme compression ratios (from 1ps to $\sim$ 10 fs) with very good peak-background contrasts. Thus, the two-pulse filamentation presents a very promising option for generating ultrashort coherent waveforms starting from relatively long-duration pulses. This option and the potential of self-compressed filaments to generate isolated attosecond pulses [26] provide an alternative route toward attosecond science [27].

The rest of the paper is organized as follows: in section 2 we discuss the basic physics underlying Cross-Phase-Modulation induced spatio-temporal reshaping. Experimental details are given in section 3 while the reader is referred to the Appendix for details on the numerical methods adopted in this work. Finally section 4 treats the nonlinear processes controlling two-pulse filamentation thus extending the results of section 2 so as to include the effects of FWM and SRS. Emphasis will also be given in this last section on the formation of temporally compressed pulses.

2. Cross-Phase-Modulation induced spatio-temporal reshaping

Before entering into the details of this work, we briefly recall the nonlinear X Wave formation, and the role self- and cross phase modulation play in it. Together with four-wave mixing processes, these are the building blocks to understand the complete picture of the two-pulse filamentation.

The notion of group velocity matching plays the central role in the X Wave formation described below. This is a general property of conical waves that makes it possible to construct localized wavepackets centered at different frequencies that nevertheless propagate with the same group velocity. This in turn leads to long effective interaction distances between different-color pulses and consequently to high efficiency of nonlinear processes.

The non-dispersive propagation characteristics of polychromatic conical waves may be expressed analytically by requiring the longitudinal component of the wave-vector, k_z, to be a linear function of the angular frequency ω, thus ensuring constant group velocity in the z direction. In a reference system centered around the pulse carrier frequency ω_0 (note that this may be either pump or seed frequency in our case), the conical wave dispersion relation may be written as

$$k_\perp = \sqrt{k^2 - k_z^2} \quad \text{with} \quad k_z = (k_0 - \beta) + (k_0' - \alpha)\Omega \,, \tag{1}$$

where $k = \omega n(\omega)/c$, $k_0 = k(\omega_0)$, k_0' is the first derivative of $k(\omega)$ evaluated at ω_0, $\Omega = \omega - \omega_0$, and the two free parameters, β and α are corrections to the phase and group velocity, respectively. The specific shape and details of the conical wave depend on the refractive index dispersion relation $n = n(\omega)$ and on the values of β and α. Typically in optical filaments in the normal GVD regime we will observe X Waves that have one of the hyperbolic tails that pass through the input pump carrier frequency at $k_\perp = 0$ so that $\beta \sim 0$ [9, 17], while the value of α, i.e. of the axial component of the group velocity $v_g = 1/(k_0' - \alpha)$, depends on the specific input conditions. We note that if we take $\beta = 0$ the second relation in Eq. (1) may be re-written as

#83915 - $15.00 USD Received 7 Jun 2007; revised 23 Jul 2007; accepted 24 Sep 2007; published 26 Sep 2007

$k_z = k_0 + \Omega/v_g$ and is formally identical to the phase matching relation of the "Effective Three Wave Mixing" (ETWM) model introduced by Kolesik et al. [39] and used to explain optical filamentation as a dynamical interaction between spontaneously formed X Waves [8, 29].

An intense laser pulse propagating in a Kerr medium will undergo a spectral broadening due to the intensity-dependence of the refractive index. In general the nonlinear material polarization may be written as $P_{NL} \propto \chi^{(3)}EEE$, where the tensor $\chi^{(3)}$ describes the Kerr nonlinearity and E is the electric field. In the presence of an intense pump field E_P and a weaker seed field E_S oscillating at frequencies ω_P and ω_S, respectively, the total field becomes $E = 1/2\{|E_P|\exp[i(k_P z - \omega_P t)] + |E_S|\exp[i(k_S z - \omega_S t)]\} + c.c.$. Substituting the total field into the relation for the nonlinear polarization and retaining only the terms that oscillate with frequency ω_S we obtain $P_{NL} \propto \chi^{(3)}(|E_S|^2 + 2|E_P|^2)E_S$. The first term describes Self-Phase-Modulation of the seed and may be neglected if the seed field is indeed weak. On the other hand the second term describes Cross-Phase-Modulation, i.e. phase modulation induced upon the weak seed wave by the intense pump wave. The material polarization wave will therefore emit an electric field that oscillates with frequency ω_S: this process may thus be viewed as a three wave scattering process in which the weak input seed field is scattered by the material polarization wave. In order to evaluate how the seed is modified we consider energy and momentum conservation. We note that the pump field, and thus the material polarization wave, may be tightly localized both in space and time as is the case for example within an ultrashort laser pulse filament. A transverse spatial dimension d implies a transverse momentum spread of the order of $\Delta k_\perp \sim \pi/d$, which in turn implies that, for a tightly localized pump pulse, transverse momentum conservation can be always satisfied [30, 31]. A similar reasoning may also be applied to the energy conservation constraint. In other words the tightly localized polarization wave may scatter a weak input seed pulse, approximated by a plane monochromatic wave with transverse wave-vector and frequency $(0, \omega_S)$, into an output wave with $(k_\perp, \omega)$ as long as $\omega - \omega_S$ is smaller than the inverse of the sub-pulse duration. Therefore, only the longitudinal k_z momentum conservation needs to be imposed explicitly and leads to:

$$K_z(\omega, k_\perp) = K_z(\omega_S, 0) - \frac{\omega_S - \omega}{v_{pol}}, \tag{2}$$

where the polarization perturbation velocity is given by the pump group velocity $v_{pol} = v_{g,p}$, and $K_z(x,y) \equiv \sqrt{(xn(x)/c)^2 - y^2}$ is a function giving the z component of the wavevector for given frequency and transverse wavenumber. The important point here is that Eq. (2) is identical to the relation in Eq. (1) (with $\beta = 0$) and we may therefore conclude that XPM tends to reshape the input Gaussian spectrum into that of a stationary conical wave. In other words, in the normal GVD regime the input Gaussian seed is expected to develop a marked conical emission (CE) pattern induced by XPM and with an angular dispersion that will support non-dispersive propagation. Furthermore, comparing Eq. (2) with Eq. (1) we observe that the XPM induced conical emission will travel at the group velocity $v_{g,p}$ of the source *pump* pulse. This may be rather surprising at first as it implies that we may arbitrarily choose the carrier frequency ω_S for the seed pulse and thus the *phase* velocity will be determined, but the *group* velocity is determined solely by the pump pulse and may be very different from both the "material" group velocities $v_{g,S} = d\omega/dk|_{\omega_S}$, $v_{g,P} = d\omega/dk|_{\omega_P}$. However, this result is completely natural and understandable once we recall that only those waveforms that satisfy Eq. (2) can be generated efficiently. These processes will be illustrated in subsection 4.1.

We note that Eq. (2) indicates that the seed pulse group velocity will not depend on frequency, i.e. the XPM-reshaped pulse will be stationary or, more precisely, it will be a stationary X Wave. This description of the X Wave formation naturally applies for either X-waves centered around seed and pump wavelength, and both are thus products of the same type of process.

#83915 - $15.00 USD Received 7 Jun 2007; revised 23 Jul 2007; accepted 24 Sep 2007; published 26 Sep 2007

The important point is that the source of energy for the seed/pump X Wave is essentially only the seed/pump pulse alone. Note however, that we have not said anything about the relation between pump and seed frequencies. If we choose the seed pulse frequency such that $\omega_S - \omega_P$ matches the SRS shift, the seed X Wave formation occurs with a drastically increased rate. In fact, the pump-depletion regime can be easily achieved [18]. The modification of the whole process in the presence of SRS resonance is such that SRS transfers the energy from the pump onto the seed pulse which in turn distributes its increased energy into the seed-centered X-wave as described above. As a result, the whole process appears to exhibit strong amplification fueled by the energy of the pump. We investigate this process in subsection 4.2.

The fact that the X Wave intensity can be enhanced by SRS opens another channel for nonlinear interactions between the seed and pump. Namely the FWM process in which photons of (now sufficiently intense) an X Wave, either seed or pump centered, are mixed with the pump or seed pulse. These higher-order processes give rise to beautiful structures in the angularly resolved spectra as described in subsection 4.3. But the really important aspect is that they can be utilized to produce extremely self-compressed pulses. We discuss this in subsection 4.4.

We have verified the scenario sketched in this section both numerically and experimentally. Numerical simulations were carried out using two different codes as described in the Appendix and that actually provide virtually identical results. The agreement between theory and experiment is extremely good as well. We can thus propose a coherent, self-consistent experimental-theoretical picture for the two-pulse filamentation in the presence of resonant energy exchange.

3. Experimental method

The experiments were carried out using a frequency-doubled Nd:glass amplified laser (Twinkle, Light Conversion Ltd., Vilnius, Lithuania) that delivers up to 4 mJ, 1 ps, 527 nm pulses with 10 Hz repetition rate. The laser pulses were loosely focused, by a 50 cm lens, down to a 90 μm FWHM diameter onto the input facet of 4 cm long fused silica cuvette containing pure water. Part of the energy of the pump pulse is split before focusing and used to pump a parametric amplifier (TOPAS, Light Conversion Ltd., Vilnius, Lithuania). The output of the amplifier after further frequency doubling is a 490 fs pulse, tunable in the 400-700 nm wavelength range. This pulse is used as the seed in our experiments: its energy is limited to 250 nJ and is focused onto the water cuvette with a larger 200 μm FWHM diameter. The temporal overlap between the pump and seed pulses is controlled by a variable delay line. The output from the water cuvette was collected with a $f = 5$ cm achromat lens. At a distance f after the lens we placed an imaging spectrometer so that at the output we recover the full (θ, λ) spectrum [7, 28]. The spectrum is then recorded by using a CCD, either a 16 bit Andor iDus or a color Nikon D70 camera that has been modified so as to extend the visibility range from 350 nm to 1100 nm [32].

In this work we refer to measurements of the spatio-temporal far-field, (θ, λ). In particular our measurements show strong and clear X shaped features, i.e. k-vector angles that increase with increasing frequency shift with respect to the on-axis pump pulse. The main point that supports our further claims is that the far-field X spectra are an indication of X Wave formation in the near field. This assumption is based on a number of observations:
(i) it has been pointed out that materials with either second order or Kerr nonlinearities may support stationary weakly localized solutions, i.e. X Waves and that a direct manifestation of these X Waves is indeed an X shape in the spatio-temporal far-field [11, 36].
(ii) The far-field spectra of stationary X Waves should have X profiles that follow a well determined law (Eq. (1)) and this has indeed been verified in many cases in Kerr media [8, 28, 29]
(iii) the X spectra clearly indicate the conical nature of the near-field pulse. Regarding the specific case of filamentation, this has been directly verified experimentally and numerically

#83915 - $15.00 USD Received 7 Jun 2007; revised 23 Jul 2007; accepted 24 Sep 2007; published 26 Sep 2007

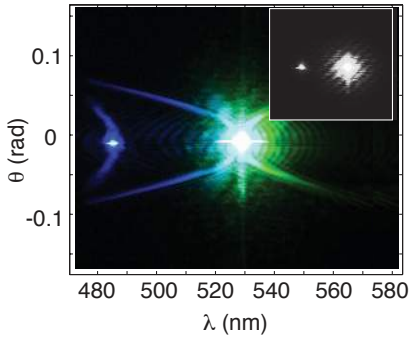

Fig. 1. Spatio-temporal modification of a weak, 250 nJ, 490 nm seed pulse in the presence of an intense, 2 μJ, 527 nm pump pulse. The inset shows the experimental spectrum taken at a lower, 1 μJ input pump energy, i.e. in the absence of nonlinear interactions.

[15, 37]. Within the assumption of cylindrical symmetry, that is suited for the modeling of single filaments, this in turn implies the existence of a non-diffracting intensity peak in the near field. This indeed is one of the most well-known and main features of optical filaments in all transparent media [1].

These points, among others, therefore sustain the claim that the observation of X shaped spectra that have cylindrical symmetry and that may also be described by Eq. 2, do indeed justify the description of the near field intensity distribution in terms of X Waves. We note that truly stationary X Waves contain infinite energy. In other words, the X Wave formation referred to in this work is considered only over a limited propagation distance (what we may refer to as the "Bessel zone") related to the finite energy actually contained within the input pump beam. These distances are usually of the order of some centimeters in condensed media and therefore sufficient for all practical purposes.

It has also been shown that the (θ, λ) spectrum may be used to determine the group velocity of a generic pulse [9, 7, 29]. For clarity we briefly describe the recipe we used for this purpose:

1. for each wavelength we take the angle θ for which maximum intensity is observed
2. using the material Sellmeier (or similar) relations for $n(\omega)$ we calculate $k = \omega n(\omega)/c$
3. we find the longitudinal wavevector from $k_z = k\sqrt{1-\theta(\omega)^2}$
4. the group velocity (along the propagation direction) may now be found from $v_g = (dk_z/d\omega)^{-1}$.

We note that the measured spectrum will always give us the external angles as the Fourier lens is surrounded by air. Therefore, when deriving the group velocity of the pulse *inside* the sample the angles must be rescaled, $\theta = \theta(\lambda) \sim \theta_{\text{measured}}(\lambda)/n(\lambda)$.

4. Nonlinear processes controlling two-pulse filamentation

4.1. XPM induced X Wave formation

Figure 1 shows the spectrum measured with a 2 μJ pump pulse and a weak 250 nJ seed pulse centered at 490 nm. The pump pulse has formed a filament within the water sample thus generating the clear blue and red-shifted CE tails that are visible around the central pump wavelength. The seed pulse also shows a clear blue-shifted CE tail. For comparison, the inset shows the same spectrum but with a lower 1 μJ pump pulse energy: the pulse has not formed a filament so that the pump peak intensity is much lower, and no nonlinear effects are taking place.

Following the recipe described above (the Sellmeier relation for water is taken from Eq. (12) in Ref. [33]) we evaluate the group velocities related to the blue-shifted CE tails originating

#83915 - $15.00 USD Received 7 Jun 2007; revised 23 Jul 2007; accepted 24 Sep 2007; published 26 Sep 2007

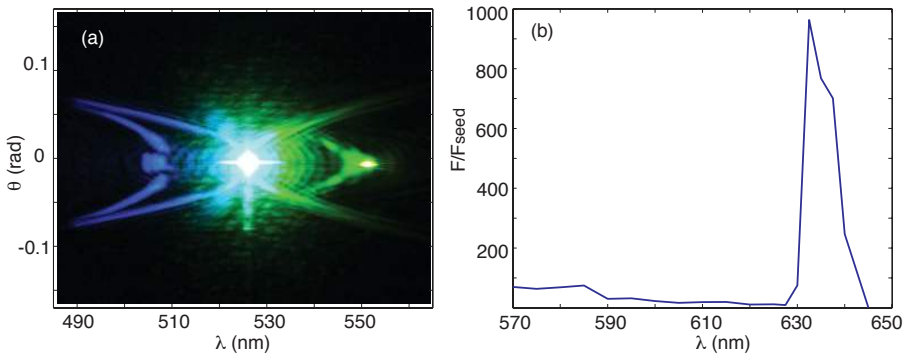

Fig. 2. (a) Experimentally measured spectrum with a 550 nm seed pulse that is reshaped into an X Wave through XPM and amplified and converted to $\sim$ 505 nm through FWM. (b) Measured peak fluence amplification of the seed pulse as the wavelength is tuned from 570 nm to 650 nm.

from the pump as $v_{g,p1} = 2.24 \pm 0.005 \times 10^8$ m/s while the red-shifted CE tails give $v_{g,p2} = 2.18 \pm 0.006 \times 10^8$ m/s. The small deviation around the mean value indicates that the group velocity has no wavelength dependence, i.e. the pulse is non-dispersive as expected for a stationary X Wave. As for the seed pulse CE, this has a group velocity $v_{g,s} = 2.26 \pm 0.06 \times 10^8$ m/s that is equal, within experimental error to $v_{g,p1}$, which may be interpreted as due to the formation of a stationary X Wave at the seed wavelength induced by XPM. We underline that this process does not necessarily require an X wave or a filament at the pump wavelength but only a very intense and tightly focused peak (although it is clear that the filament is a very practical way to achieve such conditions).

4.2. X Wave amplification through FWM and SRS

We now study the effect of tuning the seed pulse wavelength either close to the pump wavelength so as to enhance additional FWM effects through a reduction of the phase mismatch, or to the Stokes wavelength so as to enable SRS amplification.

Figure 2(a) shows an example of a spectrum measured by tuning the seed wavelength to 550 nm while input conditions for the pump are maintained as in Fig. 1. Conical emission is clearly visible originating from the seed signal and this is accompanied by the generation of a signal around 505 nm, that also exhibits marked CE. The experimentally measured pump (λ_p), seed (λ_s) and blue-shifted signal (λ_b) on-axis wavelengths are linked by the relation $1/\lambda_b = 2/\lambda_p - 1/\lambda_s$ so that we ascribe this process to FWM. Similar spectra were registered tuning the seed wavelength up to 570 nm. Once again, we evaluate the group velocities from the conical emission patterns:

$$\begin{aligned} v_{g,p1} &= 2.17 \ \pm 0.02 \ \times 10^8 \text{m/s} \quad \text{(red-shifted tails)}, \\ v_{g,p2} &= 2.236 \pm 0.005 \times 10^8 \text{m/s} \quad \text{(blue-shifted tails)}, \\ v_{g,seed} &= 2.236 \pm 0.006 \times 10^8 \text{m/s}, \\ v_{g,b} &= 2.24 \ \pm 0.01 \ \times 10^8 \text{m/s}. \end{aligned}$$

From these values we may deduce that the seed has reshaped through XPM into an X Wave that propagates with a group velocity, $v_{g,seed}$ equal to that of the superluminal pump pulse $v_{g,p2}$ and that is in turn equal (within experimental error) to the group velocity $v_{g,b}$ of the blue-shifted signal generated through FWM.

#83915 - $15.00 USD Received 7 Jun 2007; revised 23 Jul 2007; accepted 24 Sep 2007; published 26 Sep 2007

Figure 2(b) shows the gain at the seed wavelength measured as the ratio of the seed peak fluence values after and before the water cell: A gain of a factor 80 is observed over a 55 nm bandwidth. Tuning the seed further away from the pump wavelength leads to a strong reduction of the gain due to phase mismatch. However, very strong 1000× amplification is registered around 635 nm that corresponds very closely to the expected Stokes wavelength in water for a pump wavelength of 527 nm wavelength [30]. Furthermore, the gain curve around 635 nm is bell-shaped with a FWHM of ~ 200 cm^{-1} which is also in close agreement with the SRS gain bandwidth measured by other means [30]. In Ref. [7] it was shown that this amplification process is associated with the formation of so-called Raman X Waves, i.e. X Waves centered at the Stokes wavelength and amplified SRS. Furthermore it was highlighted how the Raman and pump X Waves had the same group velocity thus explaining the large SRS gain notwithstanding the short ($\tau \sim 50$ fs) pulse durations that would otherwise be expected to give rise to very short GVM walk-off lengths, $L_{GVM} = \tau \times (1/v_{g1} - 1/v_{g2})^{-1} \sim 1.8$ mm (where $v_{g1,2} = dk/d\omega|_{\omega_{1,2}}$ are the group velocities of the two pulses). It is now clear that the group velocity matching, necessary for efficient SRS amplification, is guaranteed through a XPM induced reshaping of the seed pulse into an X Wave.

Figure 3(a) shows the measured full spectrum (from the near UV to the near IR region) obtained with a 2.4 μJ input pump power and a 250 nJ seed pulse tuned to 637 nm.

The delay between the pump and seed pulse was optimized so as to maximize the intensity distribution in the CE tails around the Stokes wavelength. We note that by changing the delay within a ~ 1000 fs range it was possible to excite just the blue-shifted, red-shifted or both CE tails, in the same manner as reported in Ref. [7].

Figure 3(b) shows the numerically calculated spectrum with the same input conditions used in the experiment and simulations parameters as listed in the Appendix. In comparing with Fig. 3(a) we should bear in mind that the vertical stripe that appears only in the measured spectrum at the pump wavelength (527 nm) is due to the high pump energy illuminating the spectrometer slit which forms a highly saturated image on the CCD.

The seed pulse is retarded with respect to the pump pulse by a delay, as measured at the water cell input facet, of 600 fs. Changing the relative delay between the seed and pump pulses we were able to reproduce the "switching" between red and blue-shifted conical emission at the Stokes wavelength (data not shown). This switching mechanism was seen to depend on the seed pulse duration: with longer seed pulse durations no switching is observed while the shorter ~ 500 fs duration used in the experiment and Fig. 3(b) allows the seed to have an effective overlap with either both or with only one of the two split daughter pulses within the filament while excluding the other. In other words, by changing the delay we are able to reshape and amplify the seed pulse into two split X Waves (as in the filament) or into a single X Wave with the group velocity matched to that of the trailing or leading split pump pulse (the spectra relative to this second case are shown in Ref. [7]).

Figures 4(a) and (b) show the same spectra as in Figs. 3(a), (b) and (c) but with a higher 3.5 μJ input pump energy, highlighting once more the excellent agreement between experiment, (a), and numerics, (b) and (c), obtained with the KO and CO codes, respectively (see the Appendix for details) and indicating a certain robustness of the Raman X wave formation which was found to occur for a wide range of input parameters and working conditions. For example Fig. 5 shows another experimental spectrum obtained in 4 cm of ethanol, an input pump energy of 3.5 μJ and a 250 nJ seed pulse tuned to 623 nm (the Stokes wavelength expected for these input conditions in ethanol [30]). Here we underline the formation of two intense Raman X Waves, one at the Stokes wavelength and a second cascaded Raman X Wave at 760 nm which were measured to contain more than 50% and ~ 20% of the input pump energy, respectively.

The effect of the group velocity matching may be also appreciated in the near-field axial

#83915 - $15.00 USD Received 7 Jun 2007; revised 23 Jul 2007; accepted 24 Sep 2007; published 26 Sep 2007

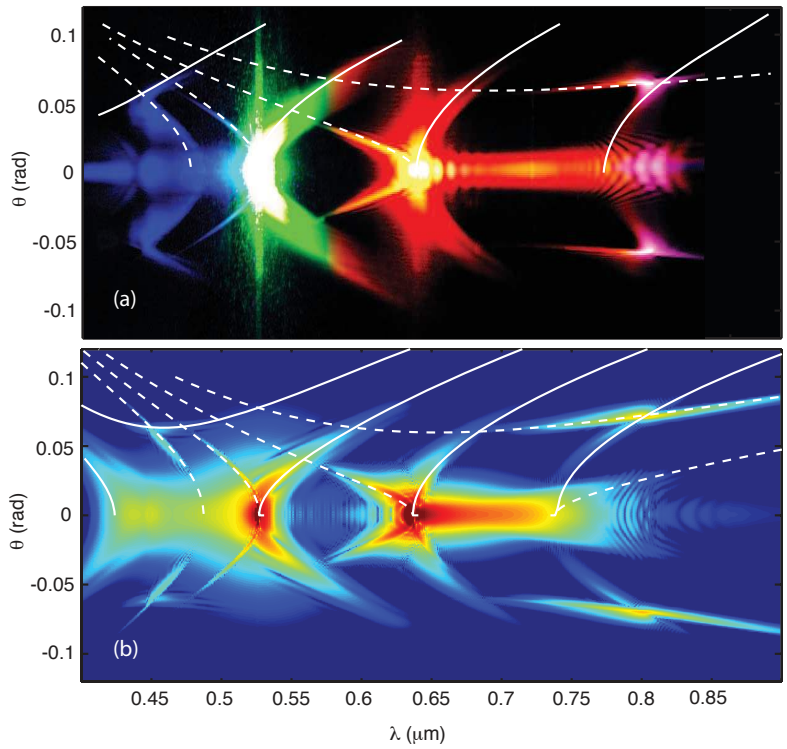

Fig. 3. (a) Measured (θ, λ) spectrum of 2.4 μJ filament in 4 cm of water with a weak 250 nJ, 637 nm seed pulse. All colors are real up to 700 nm: longer wavelengths are pink due to false color response of the modified Nikon D70 camera used for the measurement. Delay between pump and seed pulses has been optimized to maximize the intensity of X tails at the Stokes wavelength. (b) Numerical simulation (in logarithmic scale, 6 decades are shown, KO code) with the experimental input parameters in (a) and 600 fs relative delay between seed and pump pulses as measured at the water cell input facet. White lines in the graph indicate the X wave modes and related FWM curves as described in the text.

intensity profiles shown in Fig. 6 (for the same conditions as in Fig. 3). The profiles are shown for different propagation distances z as indicated in the graphs: the blue line indicates the full intensity profile and the red line shows the intensity profile of just the Stokes pulse. The input pulse splits at $z \sim 2.5$ cm into two daughter pulses that move further apart during propagation. The underlying seed pulse splits in exactly the same fashion with each seed daughter pulse remaining "locked" to the relative pump pulse. The effect of this can be clearly seen by noting that the Stokes wavelength continues to increase in energy in a steady, uniform fashion over more than 5 walk-off lengths (last graph in Fig. 6).

We also performed autocorrelation measurements in the case of water (data not shown) and these indeed indicate that pump and Raman X Waves indeed have very similar durations (within 10% deviation), as expected for the X Wave formation process induced by XPM. This finding is in agreement with numerical simulations (Fig. 6).

So our results show that the seed pulse is reshaped into an X Wave traveling at group velocity that is vastly different from the material dispersion group velocity. Although the pulse undergoes also a strong Raman amplification, robust X Wave characteristics are still maintained over the investigated propagation lengths, i.e. diffraction-free and dispersion-free propagation of the

#83915 - $15.00 USD Received 7 Jun 2007; revised 23 Jul 2007; accepted 24 Sep 2007; published 26 Sep 2007

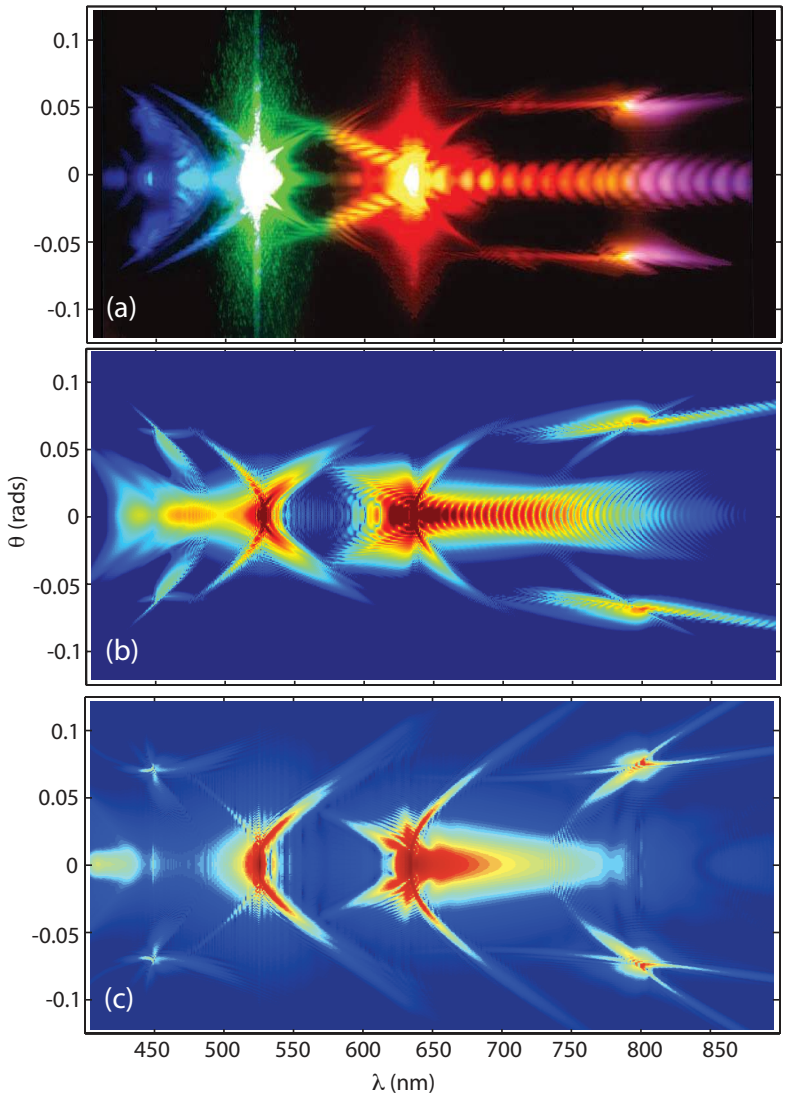

Fig. 4. Same as in Fig. 3 but with a 3.5 μJ pump pulse. (a) Experimental spectrum, (b) and (c) are the numerically simulated spectra with the KO code and CO codes, respectively.

central peak. In a loose sense this is similar to the case, or a generalization of Raman solitons that maintain their main features even in the presence of Raman amplification.

4.3. Higher-order FWM processes

We now focus our attention on the off-axis features present in all our spectra around 450 nm and 800 nm wavelengths (Figs. 3, 4 and 5). If we take for example Fig. 3(a) we note relatively intense "whiskers" of light in the red-shifted 740-820 nm region and at $\sim \pm 0.05$ rad angles. Similar "whiskers" are also visible in the blue-shifted 400-500 nm region. These features appear only in the presence of the amplified seed pulse and are thus linked to the Raman X Wave formation process. The proposed mechanism by which these "whiskers" are created is a phase

#83915 - $15.00 USD Received 7 Jun 2007; revised 23 Jul 2007; accepted 24 Sep 2007; published 26 Sep 2007

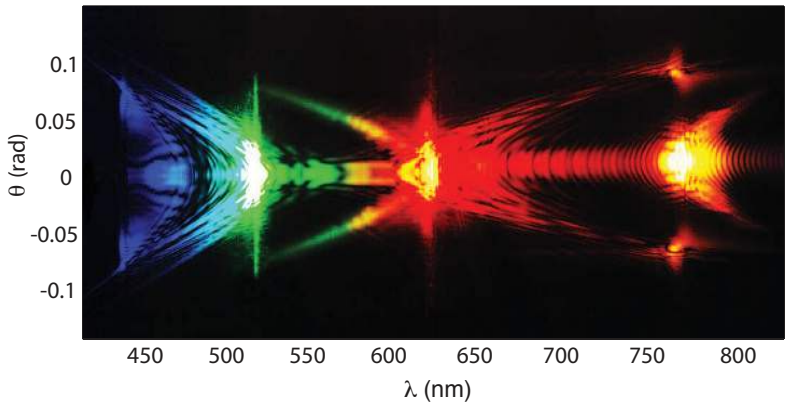

Fig. 5. Measured (θ, λ) spectrum of 3.5 μJ filament in 4 cm of ethanol with a weak 250 nJ, 623 nm seed pulse. A second-order Raman X Wave and the second-Stokes wavelength (760 nm) is observed.

matched FWM process with participation of an X Wave. We have shown that the pump and and Raman X Wave propagate with the same group velocity and overlap. This results in a beat between them which in turn serves as a "grating" that scatters the pump. Thus, two pump photons minus one X Wave photon give rise to a photon detected in the spectrum (see Fig. 7). Expressing the energy and momentum conservation for this FWM process, and eliminating the frequency and transverse wavenumber of the X Wave using its known dispersion relation, Eq. (2), we can obtain the following implicit equation for the loci of the whiskers in the $\omega, k_\perp$ space:

$$K_z(\omega, k_\perp) - 2K_z(\omega_0, 0) + K_z(\omega_S, 0) - \frac{\omega_S - 2\omega_0 + \omega}{v_g} \approx 0 \tag{3}$$

where $K_z(x,y) \equiv \sqrt{(xn(x)/c)^2 - y^2}$ is the z-component of the plane-wave's wavevector, and v represents the group velocity of one of the split-off pulses. Naturally, the same equation with exchanged role of pump and Stokes waves, $\omega_0 \leftrightarrow \omega_S$, describes a similar process in which the pump X Wave creates a beat with the Stokes wave to scatter another Stokes wave:

$$K_z(\omega, k_\perp) - 2K_z(\omega_S, 0) + K_z(\omega_0, 0) - \frac{\omega_0 - 2\omega_S + \omega}{v_g} \approx 0 \tag{4}$$

Since there are two daughter pulses after splitting, we have two possible values for v_g, namely $v_{g,1}$ and $v_{g,2}$, in each equation. Thus, we have altogether four loci around which these processes concentrate the energy in the angularly resolved spectrum. The portion of the corresponding locus that actually gets "populated" will depend on the spectral width of the pump and Stokes pulses and will correspond to the pump and Raman X Wave spectral regions that have the highest intensity.

Comparison in Fig. 3 of the loci determined by Eqs. (3) and (4) with the measured and simulated spectra confirms that these FWM processes are indeed responsible for the "whiskers". The solid lines in Fig. 3 correspond to a single value $v_g = v_{g,1,e} = 2.18 \times 10^8$ m/s for the experimental measurement (a) and to $v_g = v_{g,1,n} = 2.192 \times 10^8$ m/s for the numerical spectrum (b). The dashed lines give the pump and Raman X Waves and the "whisker" features for $v_g = v_{g,2,e} = 2.238 \times 10^8$ m/s for the experimental measurement (a) and $v_g = v_{g,2,n} = 2.23 \times 10^8$ m/s for the numerical spectrum (b). Given the overall complexity and number of physical processes involved we consider the agreement between experiment and numerics to be rather

#83915 - $15.00 USD Received 7 Jun 2007; revised 23 Jul 2007; accepted 24 Sep 2007; published 26 Sep 2007

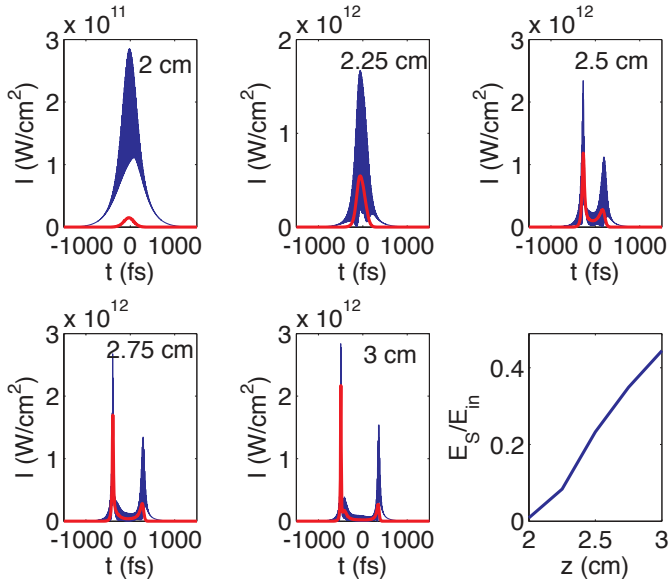

Fig. 6. Numerically simulated (CO code) on-axis temporal intensity profiles for the pump pulse (black lines) and the seed pulse (red lines). The propagation distance z is indicated in each graph. The last graph shows the Raman gain (energy at Stokes wavelength normalized to pump energy) versus z.

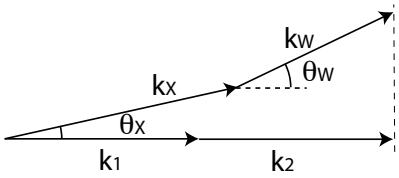

Fig. 7. Phase matching scheme used in deriving the longitudinal phase matching relations that explain the "whisker" features in the spectra. The corresponding phase matching curves are drawn as white lines in Fig. 3.

good. A further notable feature is that a single parameter is used to precisely fit simultaneously a multitude of features covering more than 400 nm bandwidth. Even small deviations of the group velocity will lead to relatively large deviations in the fit in this broad spectral range. Once the group velocity parameter has been optimized any further deviations between experiment and numerics may be ascribed to inaccuracies in the $n = n(\lambda)$ relation used in Eqs. (3) and (4). In particular we found the often used Eq. (12) from Ref. [33] to be slightly imprecise and found an overall better fit across the whole bandwidth using tabulated values as described in Ref. [39].

4.4. Wavepackets generated in FWM processes and self-compression

The understanding of the XPM induced and SRS enhanced spatio-temporal reshaping let us foresee possible applications to the production of intense visible or infrared few-cycle pulses, which constitutes the first step in the generation of intense, coherent, extreme ultraviolet sources. These sources are in turn needed to probe or trigger electron dynamics and study quantum processes in the interaction of electrons with light [40]. With a single pulse, self-

#83915 - $15.00 USD Received 7 Jun 2007; revised 23 Jul 2007; accepted 24 Sep 2007; published 26 Sep 2007

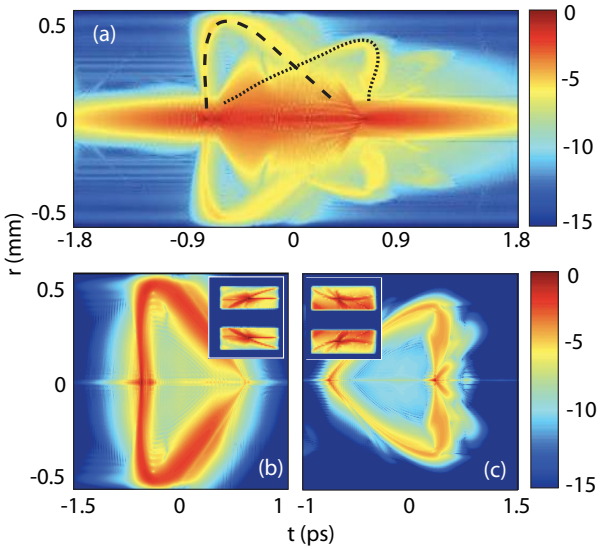

Fig. 8. Numerically simulated (CO code) near-field profiles for the spectra in normalized logarithmic scale shown in Fig. 4 . (a) the full NF profile. The dashed and dotted lines show the features associated to the red-shifted and blue-shifted "whisker" patterns, respectively. These have been isolated and are shown in (b) and (c) by filtering the full spectrum as shown in the respective insets.

compression by filamentation in gases relies on the spatiotemporal reshaping of the pulse induced by the electron plasma in the filament [22, 24] and constitutes an alternative compression technique to that of the hollow core fiber [41]. These self-compressed filaments have great potential in the generation of isolated attosecond pulses [26, 42]. With two pulse filamentation, the role of XPM effects in the self-compression process occurring in filaments was emphasized in experiments and simulations of the concatenation of two cross-polarized filaments [43]. The present results, however, allows us to propose a self-compression scheme leading to few cycle pulses with unprecedented compression ratios and an excellent temporal contrast.

In Fig. 8(a) we show the numerical near field (NF) profile of the spectrum in Fig. 4(b). In particular, we are interested in the features outlined by the dashed and dotted black lines. These features disappear when the seed is removed and are thus associated the Raman X Wave formation process. In order to investigate the origin of these weak tails we numerically performed the Fourier transform of a selected portion of the spectrum so as to obtain its near-field distribution. To this end we numerically put to zero the spectrum intensity outside the region $|0.6-1.1|$ rads, $700-900$ nm for the red-shifted whiskers and $|0.2-0.8|$ rads, $400-500$ nm for the blue-shifted whiskers. We thus found that indeed the near-field features are associated to the "whiskers" in the spectrum. In particular Fig. 8(b) shows that we are able to very cleanly isolate the leading NF tails [dashed line in Fig. 8(a)] by keeping only the red-shifted "whiskers" (as shown in the inset) while the trailing tails [dotted line in Fig. 8(a)] correspond to the blue-shifted "whiskers". The fifteen plotted decades in Fig. 8 indicate that the filtered part exhibits a potentially excellent compression ratio and temporal contrast. In Fig. 9 we consider just the on-axis ($r=0$) intensity profiles: Fig. 9(a) shows the unfiltered on-axis intensity [from Fig. 8(a)] while (b) and (c) show the on-axis intensity profiles of the red-shifted and blue-shifted "whiskers", respectively. As can be seen, these form isolated intensity peaks with ~ 15 fs and ~ 8 fs FWHM durations with very limited pre- or post-pulse oscillations and ~ 40 GW/cm^2 and ~ 200 GW/cm^2 peak intensities

#83915 - $15.00 USD Received 7 Jun 2007; revised 23 Jul 2007; accepted 24 Sep 2007; published 26 Sep 2007

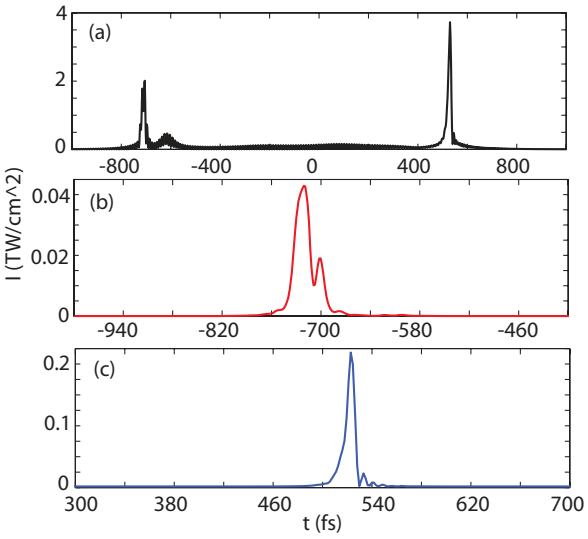

Fig. 9. Numerically simulated (CO code) on-axis temporal intensity profiles taken from Fig. 8. (a) the unfiltered profile, (b) the red-shifted "whisker" temporal profile showing a single isolated peak with $\sim$ 15 fs duration and (c) the blue-shifted "whisker" temporal profile showing a single isolated peak with $\sim$ 8 fs duration.

(corresponding to energies of 2 and 20 nJ, respectively). Such pulses could be experimentally isolated by placing an annular shaped aperture in the spatial far-field of the wave-packet.

Due to the enhancement by SRS, this pulse compression scenario based on a high order FWM process occuring in a two color filament leads to a compression factor of more than 100 (from 1 ps to 8 fs), i.e. a factor of 10 better than previously achieved by XPM effects in concatenated cross polarized filaments at the same wavelength [43]. The good contrast indicated in the simulations gives good hopes regarding a possible amplification of few cycle pulses generated by this method. Alternatively, an increase of the energy in the few-cycle structure could be achieved by working in a gas with suitable Raman parameters such as Deuterium where the same processes are expected to occur without being limited by the length of the interaction medium.

5. Conclusion

In conclusion we have shown how under conditions of extreme spatio-temporal focusing a laser pulse may reach intensities high enough to induce strong XPM effects on a much weaker seed pulse. XPM will thus induce conical emission on the seed pulse that may be interpreted as a spontaneous transformation of the seed pulse into a stationary X Wave. This finding provides an interpretation and model for those nonlinear interactions such as FWM, third harmonic generation or SRS that may occur within filaments in both condensed and gaseous media. In particular we focused attention on the case of large material gain, i.e. SRS, such that the XPM-induced seed X Wave is efficiently amplified. The large conversion efficiencies may be explained as a result of the group velocity matching between the pump and Raman X Waves. This is a unique feature of conical pulses: if the interacting pulses were Gaussian then the group velocities would be determined by the carrier wavelengths (and material dispersion at these wavelengths) and the GVM would severely limit SRS. On the other hand X Waves sustain a central intensity spike that may travel at any given group velocity and thus effectively cancel any GVM. This finding

#83915 - $15.00 USD Received 7 Jun 2007; revised 23 Jul 2007; accepted 24 Sep 2007; published 26 Sep 2007

may in principle be extended also to gaseous media: filamentation in gases leads to the formation of 10-100 TW/cm^2 intensity peaks so that, although the Raman gain is typically an order of magnitude smaller than in water, Raman X formation should maintain the same efficiency as that demonstrated in this work.

The (θ,λ) spectra also reveal the presence of FWM between the pump and Raman X Wave conical tails that leads to formation of spectrally extended "whisker" features. By isolating these features it is possible to generate ultra-short, clean $\sim 8-15$ fs pulses with pump pulse durations of 1 ps and possibly longer. Such pulses could be used for example for further amplification through Chirped Pulse Optical Parametric Amplification ([44, 45]) and generation of TW power pulses. Use of such seed pulses would imply the notable advantage of a single laser providing both high quality seed and pump pulses and thus eliminating the requirement to synchronize different laser sources.

Appendix: Numerical method

Numerical simulations were carried out using two independent codes, hereafter described as the KO-code and the CO-code.

The KO-code was written by M. Kolesik and is based on an Unidirectional Pulse Propagation Equation, the derivation of which is presented in [35, 34]. It describes the upward propagation of the spectral transverse components of the electric field $E_{\omega,k_\perp,z}$:

$$\frac{\partial E_{\omega,k_\perp,z}}{\partial z} = ik_z E_{\omega,k_\perp,z} + \frac{1}{2k_z}\left(i\frac{\omega^2}{c^2}P_{\omega,k_\perp,z} - \frac{\omega}{c^2}J_{\omega,k_\perp,z}\right) \tag{5}$$

where $k_z = \sqrt{k^2(\omega) - k_\perp^2}$. The first term on the r.h.s. of Eq. (5) describes diffraction and dispersion via a tabulated dispersion relation $k(\omega)$. Nonlinear terms are described via the polarization $P_{\omega,k_\perp,z}$ and current $J_{\omega,k_\perp,z}$. The main advantages of this formulation is that it fully accounts for nonparaxiality and captures the chromatic dispersion of the medium over an arbitrary wide frequency range.

The CO-code was written by A. Couairon and solves the nonlinear equation for the envelope $\mathscr{E}_{\omega,r,z} = \mathscr{F}(\mathscr{E}_{t,r,z})$, where $\mathscr{F}$ denotes Fourier transform and the laser field with central frequency ω_0 reads as $E_{t,r,z} = \mathscr{E}_{t,r,z}\exp(-i\omega_0 t + ik_0 z)$. The derivation of the envelope equation used in the CO-code from the wave equation in nonlinear media is recalled in Refs [1, 15].

$$\begin{aligned} 2K_g\frac{\partial \mathscr{E}_{\omega,r,z}}{\partial z} &= i\nabla_\perp^2 \mathscr{E}_{\omega,r,z} + i(k^2(\omega) - K_g^2)\mathscr{E}_{\omega,r,z} \\ &\quad + \left(i\frac{\omega^2}{c^2}\mathscr{P}_{\omega,r,z} - \frac{\omega}{c^2}\mathscr{J}_{\omega,r,z}\right) \end{aligned} \tag{6}$$

where $K_g = k_0 + k_0'(\omega - \omega_0)$. The first two terms on the r.h.s. of Eq. (6) account for diffraction in the transverse plane and dispersion described via the Sellmeier relation $k(\omega)$ given by Eq. (12) in Ref. [33], which defines the wavenumber $k_0 \equiv k(\omega_0)$, the group velocity $1/k_0' \equiv 1/(\partial k/\partial\omega)|_{\omega_0}$ and the refraction index $n_0 = k_0 c/\omega_0$. The main advantage of this formulation is that the carrier frequency does not need to be resolved, allowing a fast numerical calculation. In spite of this, Eq. (6) describes pulse propagation beyond the approximation of slowly varying temporal envelope, which is retrieved for $\omega = \omega_0$ in K_g and Eq. (6). Compared to Eq. (5), only two approximations are made: the paraxial approximation and a slightly different chromatic dispersion in the description of the nonlinear terms. Since the frequency variable in the CO-code is $\omega - \omega_0$, all explicit dependencies on ω in Eq. (6) are replaced by a function of $\omega_0 + (\omega - \omega_0)$.

#83915 - $15.00 USD Received 7 Jun 2007; revised 23 Jul 2007; accepted 24 Sep 2007; published 26 Sep 2007

In both Eqs. (5) and (6), the polarization $P_{t,r,z} = \mathscr{P}_{t,r,z}\exp(-i\omega_0 t + ik_0 z)$ describes the optical Kerr effect with coefficient n_2. It is split into an instantaneous component and a delayed (Raman-Kerr) component with fraction f_R. The polarization envelope $\mathscr{P}_{t,r,z}$ is expressed as:

$$\mathscr{P}_{t,r,z} = 2n_0 n_2 \left[\int_{-\infty}^{t} dt' R(t-t')|\mathscr{E}_{t',r,z}|^2\right] \mathscr{E}_{t,r,z} \quad (7)$$

$$R(t) = (1-f_R)\delta(t) + f_R \frac{\Lambda^2+\Gamma^2}{\Lambda} e^{-\Gamma t}\sin(\Lambda t), \quad (8)$$

and an equivalent formulation in terms of fields is obtained by replacing envelopes by the corresponding fields and $|\mathscr{E}|^2$ by $I = |E|^2$. Both the KO- and CO-codes describe multiphoton processes and plasma induced phenomena via the current and the evolution equation for the electron density:

$$\mathscr{J} = c(\sigma(\omega)\rho\mathscr{E} - n_0\beta_K|\mathscr{E}|^{2K-2}\mathscr{E}) \quad (9)$$

$$\sigma(\omega) = \sigma_r + i\sigma_i = \frac{\omega_0}{c\rho_c}\frac{\omega_0\tau_c(1+i\omega\tau_c)}{1+\omega\tau_c^2} \quad (10)$$

$$\frac{\partial\rho}{\partial t} = \frac{\beta_K}{K\hbar\omega_0}|\mathscr{E}|^{2K} + \frac{\sigma_r}{U_i}|\mathscr{E}|^2 \quad (11)$$

where β_K denotes the multiphoton absorption cross section, K the number of photons involved

Table 1. Parameters for water used in the numerical simulations

	n_2 (cm^2/W)	f_R	Γ (fs^{-1})	Λ (fs^{-1})	$\beta_K(K=3)$	U_i (eV)	τ_c (fs)
CO	3.2^{-16}	0.16	3.75×10^{-2}	0.618	1.5×10^{-24}	7.0	2
KO	2.9^{-16}	0.07	3.75×10^{-2}	0.618	1.8×10^{-23}	7.0	2

in the process, U_i the ionization potential of the medium, τ_c the collision time for the inverse Bremsstrahlung process and ρ_c the plasma density above which the medium becomes opaque at ω_0. The plasma induced dispersion in the CO-code was approximated by keeping constant $\sigma(\omega)$ in Eqs. (9,10) (evaluated at ω_0). We used the physical parameters for water in table I.

Table 2. Parameters for the input pulse and seed

	λ_0 (nm)	w_0 (μm)	τ_{FWHM} (fs)	E_{in} (μJ)	f (cm)
CO	527	100	1000	2.4–3.5	5
KO	527	100	1000	2–4	5
	λ_S (nm)	w_S (μm)	$\tau^{(S)}_{FWHM}$ (fs)	I_S (W/cm^2)	$t^{(S)}_{delay}$ (fs)
CO	637.5	150	490	2.0×10^7	$-1000 \rightarrow +1000$
KO	637.5	150	490	1.5×10^7	$0 \rightarrow +1000$

We note that the main difference between the two codes lies, not so much in the codes themselves but rather in the different approach used in modeling the water refractive index. The KO codes used a series of tabulated values ([39]) while the CO code used a commonly accepted Sellmeier relation (Eq. (12) in Ref. [33]). These small differences can be seen in Fig. 4.

The input pump and seed pulses are Gaussian in space and time with parameters in table II. Super- or sub-script "S" indicates the seed parameter, w and τ are the spatial and temporal full widths at half maximum, f indicates the focusing lens focal length while $t^{(S)}_{delay}$ indicates the range of delays tested for the seed pulse.

#83915 - $15.00 USD Received 7 Jun 2007; revised 23 Jul 2007; accepted 24 Sep 2007; published 26 Sep 2007

We also note that the parameters used in each code were tuned independently (so as to optimize agreement with the experiments) and were then finally compared to check for any evident inconsistencies. This therefore explains the differences between some of the used parameters. By choosing sets of equal parameters we did verify that the two codes continue to give practically identical results. We therefore chose to leave the original parameter values used by each code as these highlight the robustness of both the Raman X and whisker generation process.

Acknowledgments

The authors wish to acknowledge support from: the Consorzio Nazionale Interuniversitario per le Scienze della Materia (CNISM) - progetto INNESCO; the italian Ministry for Research (MIUR) - PRIN 2005; Access to Research Infrastructures activity in the Sixth Framework Programme of the EU (Contract No. RII3-CT-2003-506350, Laserlab Europe), PP acknowledges the support from Sixth EU Framework Programme Contract No. MEST-CF-2004-008048 (ATLAS), PDT acknowledges support from Marie Curie Chair project STELLA, Contract No. MEXC-CT-2005-025710. Arizona group (MK and JVM) acknowledges support from the U.S Air Force Office for Scientific Research under grant FA9550-07-1-0010. JVM acknowledges support from the Alexander von Humboldt Foundation.

#83915 - $15.00 USD Received 7 Jun 2007; revised 23 Jul 2007; accepted 24 Sep 2007; published 26 Sep 2007